Ocular Phenotype of *Fbn2*-Null Mice

Yanrong Shi,[1] Yidong Tu,[2] Robert P. Mecham,[2] and Steven Bassnett[1,2]

[1]Department of Ophthalmology and Visual Sciences, Washington University School of Medicine, St. Louis, Missouri
[2]Department of Cell Biology and Physiology, Washington University School of Medicine, St. Louis, Missouri

Correspondence: Steven Bassnett, Departments of Ophthalmology and Visual Sciences and Cell Biology and Physiology, Washington University School of Medicine, 660 S. Euclid Avenue, Campus Box 8096, St. Louis, MO 63110;
Bassnett@vision.wustl.edu.

Submitted: June 27, 2013
Accepted: September 20, 2013

Citation: Shi Y, Tu Y, Mecham RP, Bassnett S. Ocular phenotype of *Fbn2*-null mice. *Invest Ophthalmol Vis Sci*. 2013;54:7163–7173. DOI:10.1167/iovs.13-12687

Purpose. Fibrillin-2 (*Fbn2*) is the dominant fibrillin isoform expressed during development of the mouse eye. To test its role in morphogenesis, we examined the ocular phenotype of $Fbn2^{-/-}$ mice.

Methods. Ocular morphology was assessed by confocal microscopy using antibodies against microfibril components.

Results. $Fbn2^{-/-}$ mice had a high incidence of anterior segment dysgenesis. The iris was the most commonly affected tissue. Complete iridal coloboma was present in 37% of eyes. Dyscoria, corectopia and pseudopolycoria were also common (43% combined incidence). In wild-type (WT) mice, fibrillin-2-rich microfibrils are prominent in the pupillary membrane (PM) during development. In *Fbn2*-null mice, the absence of *Fbn2* was partially compensated for by increased expression of fibrillin-1, although the resulting PM microfibrils were disorganized, compared with WTs. In colobomatous adult $Fbn2^{-/-}$ eyes, the PM failed to regress normally, especially beneath the notched region of the iris. Segments of the ciliary body were hypoplastic, and zonular fibers, although relatively plentiful, were unevenly distributed around the lens equator. In regions where the zonular fibers were particularly disturbed, the synchronous differentiation of the underlying lens fiber cells was affected.

Conclusions. *Fbn2* has an indispensable role in ocular morphogenesis in mice. The high incidence of iris coloboma in *Fbn2*-null animals implies a previously unsuspected role in optic fissure closure. The observation that fiber cell differentiation was disturbed in $Fbn2^{-/-}$ mice raises the possibility that the attachment of zonular fibers to the lens surface may help specify the equatorial margin of the lens epithelium.

Keywords: pupillary membrane, tunica vasculosa lentis, coloboma, ciliary zonule, lens, ciliary epithelium, optic fissure, fibrillin

Fibrillins are large, cysteine-rich glycoproteins found in the extracellular matrix of force-bearing structures such as ligaments, blood vessels, and lungs.[1] The human genome contains three fibrillin genes (*FBN1-3*) but in mice the *Fbn3* gene appears to be inactive.[2] Fibrillin monomers are arranged head-to-tail, forming characteristic 10- to 12-nm-diameter microfibrils.[3] In some tissues, fibrillin is found at the periphery of elastic fibers, acting as a scaffold for elastin deposition. In other structures, notably the ciliary zonule of the eye, fibrillin is found in elastin-free assemblies.

In humans, mutations in *FBN1* underlie Marfan syndrome (MFS; Mendelian Inheritance in Man [MIM]: 154700), an autosomal dominant condition characterized by tall stature and often serious cardiovascular complications. The eye is also commonly affected in MFS.[4] Ocular manifestations include ectopia lentis, axial myopia, and microspherophakia. Mutations in *FBN2*, on the other hand, result in congenital contractural arachnodactyly (CCA; MIM: 121050), also known as arthrogryposis distal type 9, Beals syndrome, or Beals-Hecht syndrome.[5] CCA is a rare autosomal dominant connective tissue disorder characterized by arachnodactyly (long, thin digits), joint contractures, scoliosis, and crumpled ears. When first described in the 1970s, CCA was considered clinically distinct because the cardinal ocular and cardiovascular features of MFS appeared to be absent. More recent reports, however, suggest considerable phenotypic overlap between the two syndromes. Cardiovascular involvement in CCA can include mitral valve prolapse and aortic root enlargement.[6] Although ocular symptoms appear less ubiquitous in CCA than in MFS, several ophthalmological case reports have noted the sporadic occurrence of anterior segment pathology in CCA patients including megalocornea,[7] keratoconus,[6,8] iridodonesis,[7] ectopia lentis,[9] iris[10,11] and lens[12] coloboma, ciliary body hypoplasia,[12] and high myopia.[12–17]

Radiation-induced and spontaneous mutations in *Fbn2* have been identified in mice. The classic shaker-with-syndactylism mutation, *sy*, was the first to be identified in the 1940s.[18] Induced by irradiation, *sy* was eventually shown to result from the deletion of an approximately 0.7-cM region of mouse chromosome 18.[19] The deleted region contained two genes, *Slc12a2* and *Fbn2*. Deletion of *Slc12a2* accounted for the neurological component of the *sy* phenotype, while loss of *Fbn2* was responsible for syndactylism (fused digits).[20,21] In addition to *sy*, two spontaneous mutant alleles ($Fbn2^{fp}$ and $Fbn2^{fp\text{-}2J}$),[21] an allele ($Fbn2^{Mz}$) identified in a large scale N-ethyl-N-nitrosourea mutagenesis screen,[22] and an allele ($Fbn2^{fp\text{-}3J}$) induced by chemical mutagenesis in ES cells[23] have been reported. Finally, a null allele ($Fbn2^{-/-}$) was generated by gene targeting in embryonic stem cells.[24] It is probable, in all cases, that little or no functional Fbn2 protein was produced.[22] The most consistently reported phenotype in the *Fbn2* mutants was syndactyly, which was usually bilateral,

affecting hind-limbs and/or fore-limbs. Additionally, $Fbn2^{-/-}$ animals were found to have temporary contractures of carpal, metacarpal, and phalangeal joints, reminiscent of the clinical presentation of CCA in human neonates.[24] Careful analysis of muscle strength in $Fbn2^{Mz}$ and $Fbn2^{fp}$ mice revealed weakness of skeletal muscles,[22] again reminiscent of patients with CCA, who commonly present with muscle hypoplasia and weakness. Thus, extant mouse models recapitulate some, but by no means all, aspects of the CCA phenotype in humans.

The expression of *Fbn1* and *Fbn2* was recently examined in the wild-type (WT) mouse eye.[25] In situ hybridization analysis indicated that *Fbn2* was strongly expressed during embryonic ocular development. Fbn2-rich microfibrils were particularly abundant in the pupillary membrane (PM) and tunica vasculosa lentis, which, together, constitute the temporary vascular tunic that nourishes the developing lens. By embryonic day 16 (E16), the periocular mesenchymal cells and cells at the anterior margin of the inner layer of the optic cup (the presumptive nonpigmented ciliary epithelium [NPCE]) also expressed *Fbn2* strongly. In comparison, *Fbn1* expression was relatively modest in the embryonic eye, although a marked increase in postnatal expression of *Fbn1* in the NPCE was noted. Due to the concomitant waning of *Fbn2* expression postnatally, *Fbn1* was the dominant fibrillin transcript in mouse NPCE cells by 1 month of age.

Although no ocular phenotype has been reported for any of the mouse *Fbn2* mutants, the expression pattern of *Fbn2* in the embryonic WT mouse eye strongly suggested a role for *Fbn2* in ocular development. To test this hypothesis, we examined the eyes of $Fbn2^{-/-}$ mice. Our data identify a previously unsuspected role for *Fbn2* in anterior segment development and, further, suggest that mouse models may prove useful in studying the ocular complications of fibrillinopathies.

Materials and Methods

Animals

The generation of $Fbn2^{-/-}$, $Mfap2^{-/-}$, and $Mfap5^{-/-}$ mice was described previously.[24,26,27] Knockout animals were maintained on a mixed C57BL/6Jx129Sv background; 129Sv and C57BL/6J animals were obtained commercially (Jackson Lab, Bar Harbor, ME) and used as WT controls. Mice (109 in total) were examined from postnatal day 1 (P1) to 10 months of age. To assess the gross ocular phenotype, mice were anesthetized with a cocktail of ketamine (80 mg/kg) and xylazine (6 mg/kg) and examined using a stereomicroscope. The cornea was moistened with a drop of PBS during observation. Mice were examined for the presence of coloboma (notched iris), corectopia (off-center pupil), dyscoria (misshapen pupil), and pseudopolycoria (fenestrated/hypoplastic iris). The examination was conducted by two investigators who were not masked as to genotype. The pupil light response was evaluated using a fiberoptic illuminator (ACE EKE Schott light source; Advanced Imaging Concepts, Inc., Princeton, NJ) positioned 20 cm from the eye.

To examine the internal structure of the eye, mice were killed by CO_2 inhalation. Eyes were enucleated and processed for immunofluorescence experiments or lens shape measurements, as described below. All procedures described herein were approved by the Washington University Animal Studies Committee and were performed in accordance with the ARVO Statement for the Use of Animals in Ophthalmic and Vision Research.

Immunofluorescence

Enucleated eyes were fixed overnight in 4% paraformaldehyde/PBS. The fixed tissue was rinsed in PBS and then dissected to remove the posterior globe to the level of the pars plana. Anteriorly, the cornea and iris were carefully removed. Dissected specimens thus consisted of scleral rings with attached ciliary zonules and lenses. Nonspecific antibody binding was minimized by a 2-hour incubation in blocking solution containing 5% bovine serum albumin (BSA) in PBS. Samples were incubated overnight at 4°C in primary antibody diluted (1:50) in 2.5% BSA/PBS. After thorough washing in PBS, samples were incubated with appropriate fluorescently labeled secondary antibodies for 2 hours at room temperature. After final washing, samples were imaged by confocal microscopy, using a glass-bottomed viewing chamber, as described.[28]

Antibodies

Anti-mouse fibrillin-1 was generated as described[29] and generously provided by Lynn Sakai, Oregon Health Science University, Portland, OR. Goat polyclonal anti-MAGP1 was obtained from a commercial supplier (Cat # sc-50084; Santa Cruz Biotechnology, Inc., Santa Cruz, CA). The specificity of this antibody was demonstrated previously using ocular tissues from $Mfap2^{-/-}$ mice.[25] Blood vessels were visualized using a monoclonal antibody (Clone 2H8) against CD31 (platelet endothelial cell adhesion molecule 1 [PECAM1]), an integral membrane protein enriched at vascular endothelial cell junctions (Cat # MAB1398Z; Millipore, Billerica, MA). Alexa488-conjugated chicken anti-goat and chicken anti-rabbit, and Alexa543- and Alexa633-conjugated donkey anti-rabbit were obtained commercially (Invitrogen, Grand Island, NY) and used in appropriate combinations with the primary antibodies.

Lens Shape Analysis

Lens clarity was assessed by photographing the tissue against a grid pattern.[30] To measure the curvatures of the refractive surfaces, lenses were dissected from the eye and placed in a spectrophotometer cuvette containing warm tissue culture medium supplemented with 20% density gradient medium (Percoll; GE Healthcare Bio-Sciences, Piscataway, NJ), as described.[31] In such a medium, lenses have near-neutral buoyancy and their shapes are not, therefore, distorted under their own weight. Lenses were photographed in profile through a 45° glass prism positioned next to the cuvette. The size and shape of the lenses were determined from calibrated digital images using Metamorph image analysis software (V. 7.7; Molecular Devices, Sunnyvale, CA). Only lenses from male animals were used, to control for possible sex differences in lens size.

Imaging

Confocal data sets were collected using a Zeiss 510LSM META confocal microscope in the inverted configuration (Carl Zeiss, Thornwood, NY). Stacks of optical sections were visualized as maximum intensity orthographic projections or rendered in three dimensions using the Simulated Fluorescence Process (SFP) volume renderer (Scientific Volume Imaging, Hilversum, The Netherlands).

Results

Gross Phenotype

A proportion of the $Fbn2^{-/-}$ mice (≈25%) exhibited syndactyly, with fusion of the third and fourth digits (Supplementary

Investigative Ophthalmology & Visual Science

Table. Ocular Phenotypes in Adult (1–10 Months Old) WT and Mutant Mice

Genotype	No. Eyes Examined	Normal Appearance	Corectopia/Dyscoria	Iridal Coloboma
C57BL/6J (WT)	15	15	0	0
*129*Sv (WT)	16	16	0	0
Fbn2$^{-/-}$	101	20	44	37
Fbn2$^{-/-}$; *Mfap2*$^{-/-}$	27	2	9	16
Mfap2$^{-/-}$	16	16	0	0
Mfap5$^{-/-}$	10	10	0	0
Mfap2$^{-/-}$; *Mfap5*$^{-/-}$	12	12	0	0

Mice deficient in *Fbn2* were prone to iris malformations including corectopia, dyscoria, and coloboma. Mice deficient in *Mfap2* and *Mfap5* (genes encoding microfibril-associated glycoproteins) did not exhibit ocular symptoms.

Fig. S1, Supplementary Table S1), in accord with earlier observations.[21,22,24] We also noted occasional newborns with fore- and/or hind-limb joint contractures that eased in the immediate postnatal period, as described.[24] At 2 weeks of age, *Fbn2*$^{-/-}$ mice were indistinguishable in weight from age-matched WTs (C57BL/6J) but, by 3 months of age, were significantly smaller (Supplementary Fig. S2).

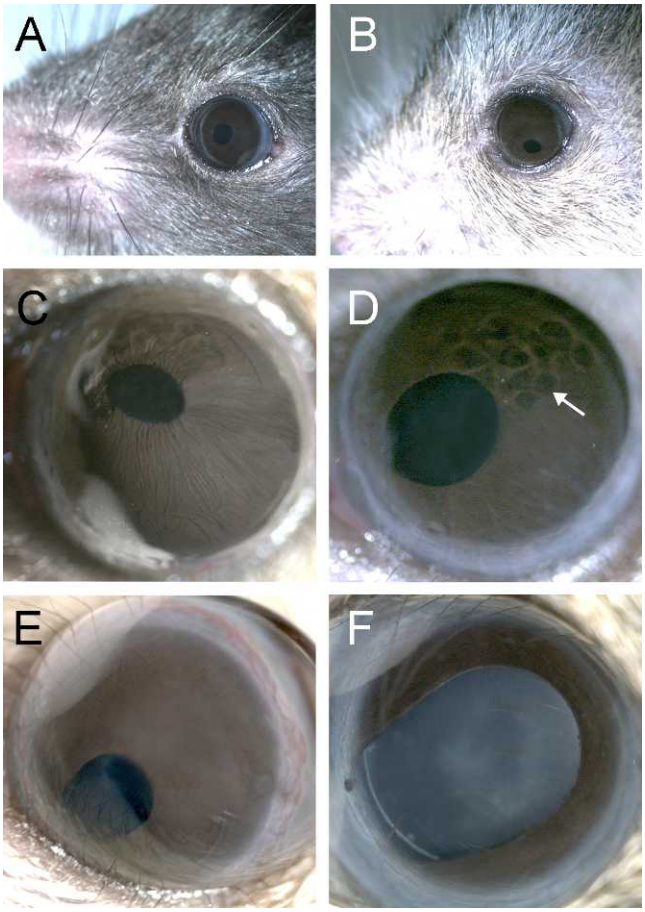

Figure 1. Iris malformations in *Fbn2*-null mice. In WT mice, the pupil is circular and properly centered (**A**). *Fbn2*-null mice exhibited a range of iris defects including corectopia (**B**), dyscoria (**C**), iris hypoplasia/pseudopolycoria (*arrowed* in [**D**]), and typical coloboma (**E**). Mice deficient in both *Fbn2* and *Mfap2* generally exhibited more severe iris phenotypes (**F**). The mice shown are 1 to 2 months old except for (**B**) and (**D**), which are 10 months old.

Ocular Phenotype

The external ocular phenotype was assessed by stereomicroscopy in anesthetized animals. In addition to C57BL/6J and 129Sv mice (the background strains for the *Fbn2*$^{-/-}$ animals), we also examined mice deficient in the microfibril-associated glycoproteins, Mfap2 and Mfap5 (aka Magp1 and Magp2, respectively), as well as two compound mutants (*Fbn2*$^{-/-}$; *Mfap2*$^{-/-}$ and *Mfap2*$^{-/-}$; *Mfap5*$^{-/-}$). External eye size and shape were qualitatively indistinguishable between WT strains and the various mutants. Within the eye, however, it was apparent that most (≈80%) of the *Fbn2*$^{-/-}$ mice had abnormal irides (Table). Corectopia (off-center pupil), dyscoria (misshapen, generally oval or tear-drop, pupils), and iris coloboma were all noted (Fig. 1). Iris abnormalities were not observed in C57BL/6 or 129Sv background strains or in mice deficient in *Mfap2* or *Mfap5* (alone or in combination). Although the phenotype of double knockout (*Fbn2*$^{-/-}$; *Mfap2*$^{-/-}$) mice was not examined exhaustively, the proportion of eyes with iridal coloboma (16/27; 59%) and the severity of the phenotype, appeared greater in that compound mutant than in mice deficient in either *Fbn2* (37%) or *Mfap2* (0%) alone (see Figs. 1E, 1F). Corectopic pupils were usually displaced inferiorly (Fig. 1B). Similarly, iris colobomata were most often located in the inferior quadrant (Figs. 1E, 1F). In older mice (>6 months), iris hypoplasia was also occasionally noted, leading to a pseudopolycoria phenotype (arrowed in Fig. 1D). Colobomata were present in 37% of *Fbn2*$^{-/-}$ eyes. These were classified as "typical" colobomata, as the term is understood clinically, meaning that the iris defect was aligned with the axis of the embryonic optic fissure. Most of the colobomata were complete, extending from the border of the pupil to the margin of the ciliary epithelium. In colobomatous eyes, the lens equator could often be observed through the notched portion of the iris (Fig. 1F).

The pupil light response reflex was evaluated in anesthetized, 2-month-old *Fbn2*$^{-/-}$ mice with corectopia. In such animals, the pupil constricted normally under bright light conditions (Fig. 2A). However, miosis was not sustained. After 5 minutes under constant bright light, the pupil dilated (Fig. 2B) and was unresponsive to further stimulation. Under the same illumination conditions, miosis was sustained in WT mice (Figs. 2C, 2D).

In humans, ectopia lentis is a common feature of fibrillinopathies, such as MFS and autosomal dominant Weill-Marchesani syndrome. Ectopia lentis et pupillae (combined mislocalization of the lens and the pupil) is a related condition, resulting from mutations in ADAMTSL4.[32] Consequently, *Fbn2*$^{-/-}$ mice were examined carefully for signs of dislocated lenses. In rodents, the lens occupies most of the intraocular volume and, as a result, a dislocated lens might go undetected on external examination. Therefore, we fixed the eyes and

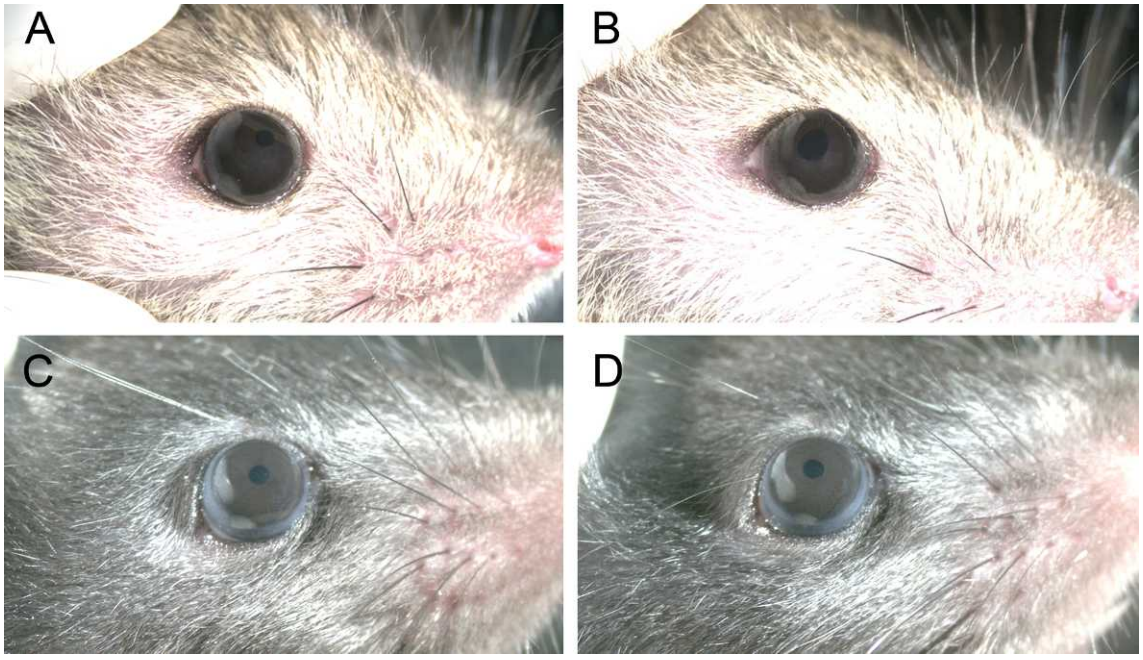

Figure 2. Failure to sustain light-induced pupillary constriction in 2-month-old *Fbn2*$^{-/-}$ mice. In *Fbn2*$^{-/-}$ mice, corectopic pupils constrict initially in response to bright light (**A**). After 5 minutes in constant bright light, however, the pupil dilates (**B**), becoming unresponsive to further fluctuations in light intensity. Under the same illumination conditions, constriction is maintained in a WT mouse (**C**, **D**). Images are representative of six independent experiments.

removed the posterior wall of the globe to visualize the in situ orientation of the lens. In fixed tissue, the Y-shaped lens sutures on the anterior and posterior lens faces were clearly visible. The sutures mark the point of convergence of lens fiber cell tips at the anterior and posterior poles of the lens and may thus be used to visualize the lens optical axis. We found that the lens axis was always properly oriented in the eye, irrespective of the position, size, or shape of the pupil (data not shown). Thus, there was no evidence of frank lens dislocation in *Fbn2*$^{-/-}$ mice, despite the presence of severe iris malformations.

Effects on the PM

Previously, we reported that *Fbn2* was the dominant fibrillin isoform during early eye development.[25] In situ hybridization experiments demonstrated that *Fbn2* was expressed strongly by capillary endothelial cells in the temporary vasculature (PM, anteriorly; and tunica vasculosa lentis, posteriorly) surrounding the developing WT lens. Consistent with this observation, PM microfibrils were found to be particularly enriched in Fbn2 protein, with comparatively low levels of Fbn1.[25] We examined the PM in eyes from P1 *Fbn2*$^{-/-}$ mice, to determine whether the absence of *Fbn2* affected the organization or composition of the microfibril network or the disposition of the associated capillary bed (Fig. 3). The distribution of microfibrils was visualized using an antibody against the microfibril-associated protein, Magp1 (Fig. 3A). At low magnification, the characteristic anastomosing pattern of PM capillaries was evident in Magp1-stained WT samples (Fig. 3A). In contrast, the microfibril network in the PM of *Fbn2*$^{-/-}$ animals was so disorganized that it was difficult to discern the organization (or even existence) of the underlying capillaries. The distribution of individual WT or *Fbn2*-deficient microfibrils and their relationship to the PM capillaries was analyzed at higher magnification (Fig. 3B). Capillaries were visualized directly using antibodies against CD31, an endothelial cell marker. In WT animals, microfibrils were evenly spaced and most were located in the gaps between neighboring capillaries. In contrast, *Fbn2*$^{-/-}$ microfibrils formed disorganized fiber aggregates, many of which extended over, rather than between, capillaries. However, although disorganized, Magp1-positive microfibrils remained plentiful in the PM of *Fbn2*$^{-/-}$ mice (Figs. 3A, 3B). To determine whether *Fbn1* expression was increased in the absence of *Fbn2*, we double-labeled PMs from WT or *Fbn2*$^{-/-}$ mice with anti-Magp1 and anti-Fbn1 (Fig. 3C). Magp1 staining intensity was comparable between the two genotypes. In WT PMs, microfibrils contained relatively low levels of Fbn1, as noted previously.[25] However, in *Fbn2*-null animals, the level of Fbn1 in PM microfibrils was markedly increased. Thus, in *Fbn2*$^{-/-}$ mice, the absence of Fbn2 was accompanied by increased Fbn1 immunofluorescence in PM microfibrils.

Effects on the Optical Aperture of the Eye

In mice, the iris does not develop until after birth. Thus, in neonatal animals, the optical aperture of the eye is defined not by the pupil diameter but, rather, by the diametric distance from one rim of the ciliary body to the opposite rim. In the course of our immunofluorescence experiments, we noted that the optical aperture often appeared larger in the *Fbn2*$^{-/-}$ animals than in age-matched WT controls (compare, e.g., the images shown in Fig. 3A). Quantitative measurements (Fig. 4) confirmed that, at P1, the aperture in *Fbn2*$^{-/-}$ eyes (932 $\pm$ 59 μm; mean $\pm$ SD, $n = 8$) was significantly larger than WTs (741 $\pm$ 59 μm; $n = 10$, $P < 0.001$).

Iridal Coloboma in *Fbn2*$^{-/-}$ Mice Is Associated With a Persistent PM

We examined colobomatous eyes in greater detail by confocal microscopy, using anti-Magp1 to visualize the distribution of microfibrils. In WT mice, the PM usually regresses over the first

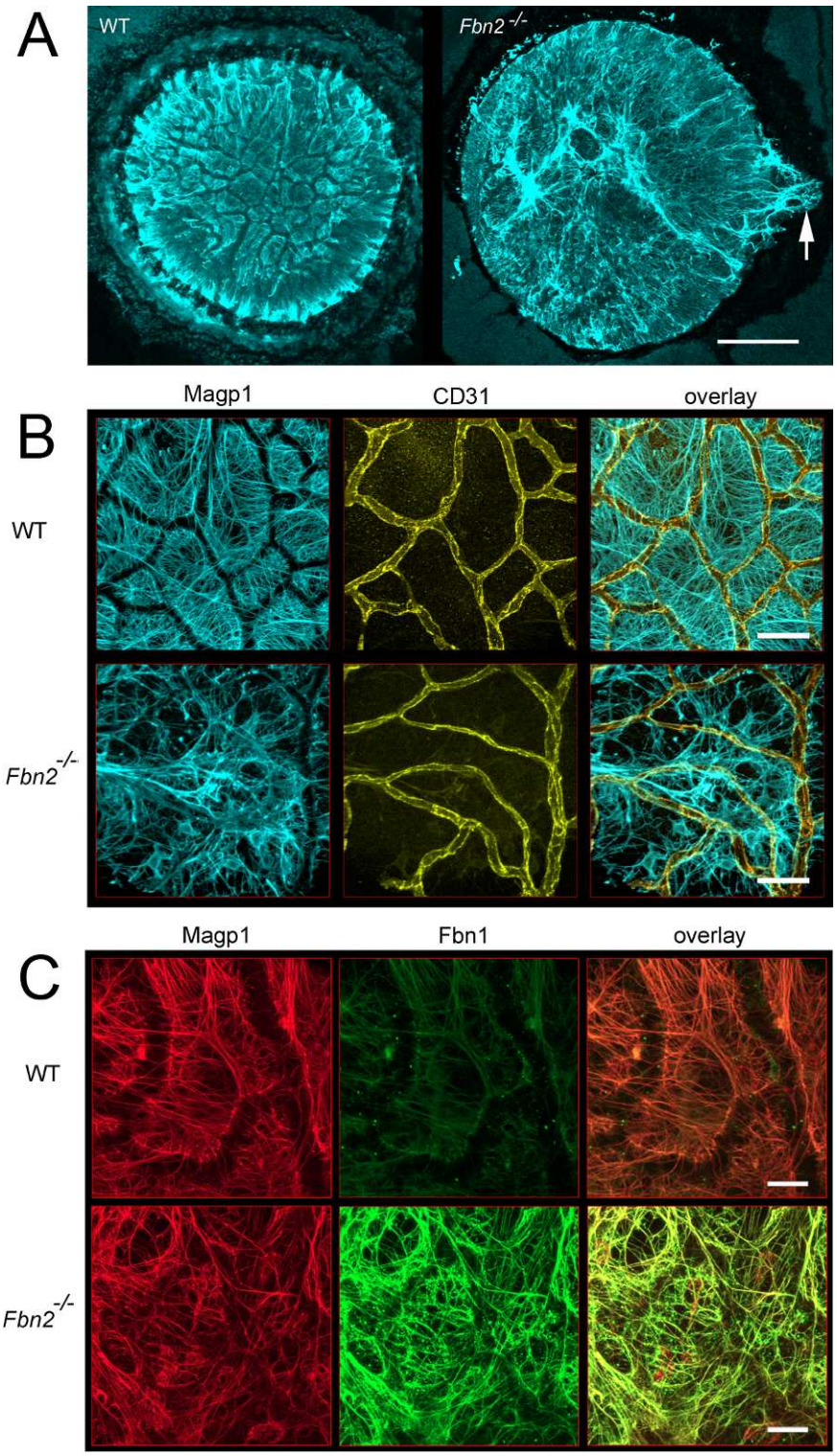

Figure 3. Arrangement of microfibrils and capillaries in the PM of WT and *Fbn2*$^{-/-}$ mice at P1. (**A**) In WT mice, microfibrils (visualized using anti-Magp1; *light blue*) are abundant in the PM and the anastomosing pattern of vessels in the associated capillary bed is revealed by gaps in the Magp1 immunofluorescence. In contrast, microfibrils in the *Fbn2*$^{-/-}$ PM are disorganized and capillaries are not visible. The position of a coloboma is indicated by the *arrow*. (**B**) The spatial relationship between microfibrils and capillaries is disturbed in the PM of *Fbn2*$^{-/-}$ animals. In WT mice, evenly spaced microfibrils (visualized with anti-Magp1; *light blue*) are plentiful in the spaces between adjacent capillaries (visualized with anti-CD31; *yellow*). In contrast, microfibrils are disorganized and aggregated in the *Fbn2*$^{-/-}$ PM and often project over the capillary elements. (**C**) *Fbn1* expression in the PM is enhanced in the absence of *Fbn2*. Microfibrils in the PM were visualized using anti-Magp1 (*red*) or anti-Fbn1 (*green*). In the absence of Fbn2, Fbn1 immunofluorescence is markedly increased. In each case, images are representative of at least six independent experiments. *Scale bars*: (**A**) 250 μm, (**B**) 50 μm, (**C**) 25 μm.

Investigative Ophthalmology & Visual Science

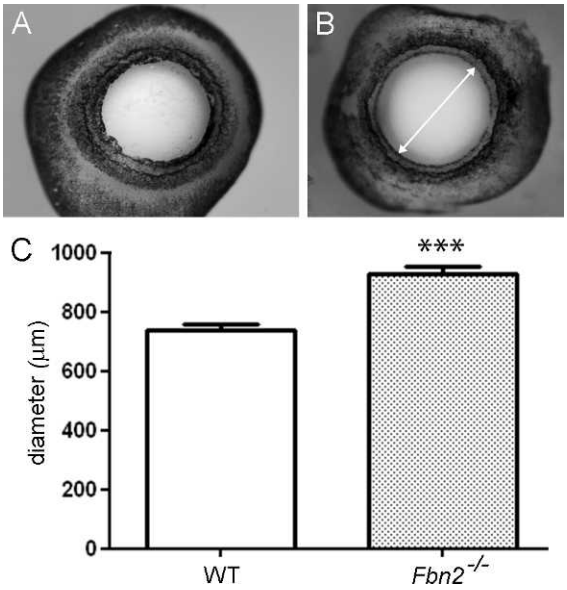

Figure 4. Ocular aperture is significantly increased in P1 *Fbn2*$^{-/-}$ mice. The ocular aperture is the diametric distance from the ciliary process on one side of the eye to the other (*arrowed* in [**B**]). The aperture was consistently smaller in WT eyes (**A**) than in *Fbn2*$^{-/-}$ eyes (**B**). Quantitative data in (**C**) represent mean ± SD (wild type $n = 10$; *Fbn2*$^{-/-}$ $n = 8$). ***$P < 0.001$ (two-tailed *t*-test).

2 postnatal weeks and is completely absent from adult animals.[33] In contrast, adult *Fbn2*$^{-/-}$ eyes invariably retained vestiges of the PM (Fig. 5). In colobomatous *Fbn2*$^{-/-}$ eyes, a persistent PM covered the region of the anterior lens surface closest to the notch in the iris (Fig. 5A). Blood vessels (the identities of which were verified at high magnification; see Supplementary Fig. S3) were integrated into the persistent PM. Eyes with partial coloboma were less severely affected (Fig. 5B), although Magp1-positive, irido-lenticular adhesions often connected the edge of the pupil to the lens surface.

Ciliary Body Hypoplasia in *Fbn2*$^{-/-}$ Mice

Scanning electron microscopy has previously revealed that the murine ciliary epithelium is arranged in a series of somewhat irregular, radially oriented folds.[34] This arrangement was confirmed in three-dimensional confocal reconstructions of the ciliary body from WT mice (Fig. 6A). In *Fbn2*$^{-/-}$ mice, however, en face confocal reconstructions of the entire ciliary epithelium revealed that segments of the epithelium were hypoplastic. In these regions, the ciliary body was thinner and the epithelium less elaborately folded than in WT (Fig. 6B). Furthermore, in the hypoplastic regions the folds were oriented circumferentially rather than radially.

Ciliary Zonule Organization and Lens Fiber Differentiation in *Fbn2*$^{-/-}$ Eyes

The lens is suspended from a complex, fibrous rigging called the ciliary zonule. In mice, the zonule is synthesized by cells of the NPCE and composed primarily of Fbn1, Fbn2, and Magp1.[25] We examined the three-dimensional organization of the ciliary zonule in WT mice and found it to be similar to that reported previously.[25] Namely, zonular fibers extended from the posterior portion of the pars plicata, to attachment points near the lens equator (Figs. 7A, 7C). The posterior zonular fibers attached to the lens at the fibrillar girdle (arrowed in Fig. 7A), a dense meshwork of radially oriented microfibrils associated with the capsular surface. The fibrillar girdle encircled the lens near the equatorial margin of the epithelium. Although zonular fibers were plentiful in the eyes of *Fbn2*$^{-/-}$ mice (Figs. 7B, 7D–F), they were much less regularly arranged than in WT animals. In *Fbn2*$^{-/-}$ eyes, the attachment points of the posterior zonular fibers were displaced posteriorly on the lens capsule. The differentiation of lens epithelial cells into lens fiber cells is normally closely synchronized. As a result, in WT lenses, the nuclei of the differentiating fiber cells fall on a single line of latitude (see Fig. 7A). In some *Fbn2*$^{-/-}$ eyes, the ciliary zonule was particularly disturbed (see, e.g., Figs. 7E, 7F). In such cases, the lens fiber cell nuclei were not arrayed along a single latitudinal line. The resulting undulations in the

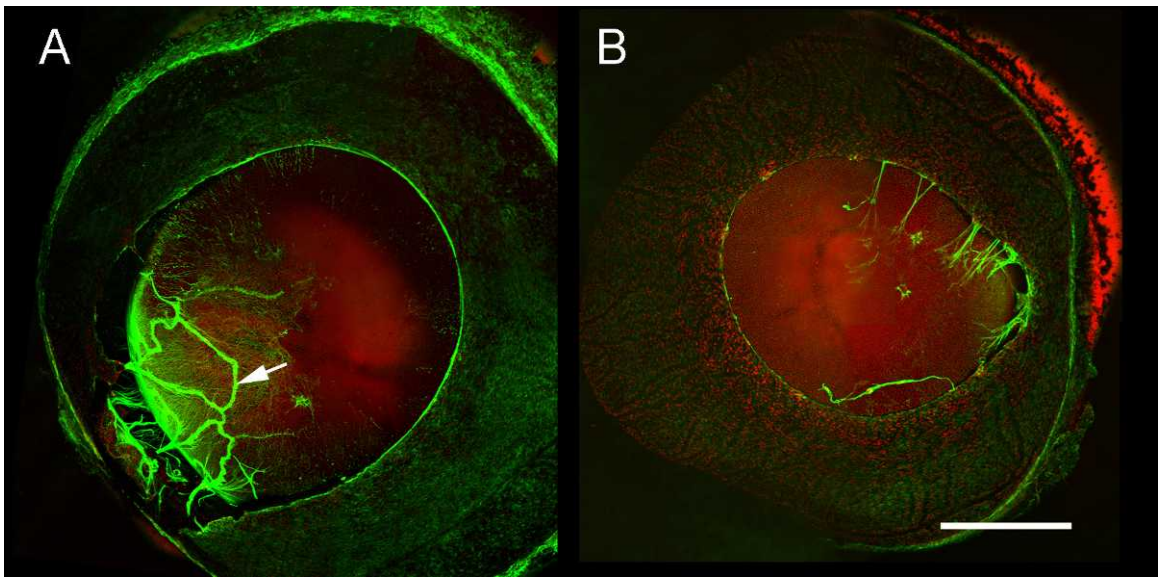

Figure 5. Persistent PM in adult *Fbn2*$^{-/-}$ mice with complete (**A**) or partial (**B**) iridal coloboma. Microfibrils (*green*) are labeled with anti-Magp1. Nuclear DNA (*red*) is labeled with Draq5. A persistent PM is associated with notched region of the iris (**A**). Within the PM, Magp1-positive capillaries are evident (*arrow*). In the partial coloboma (**B**), Magp1-positive adhesions link the margin of the iris to the underlying lens capsule. *Scale bar*: 500 μm.

Investigative Ophthalmology & Visual Science

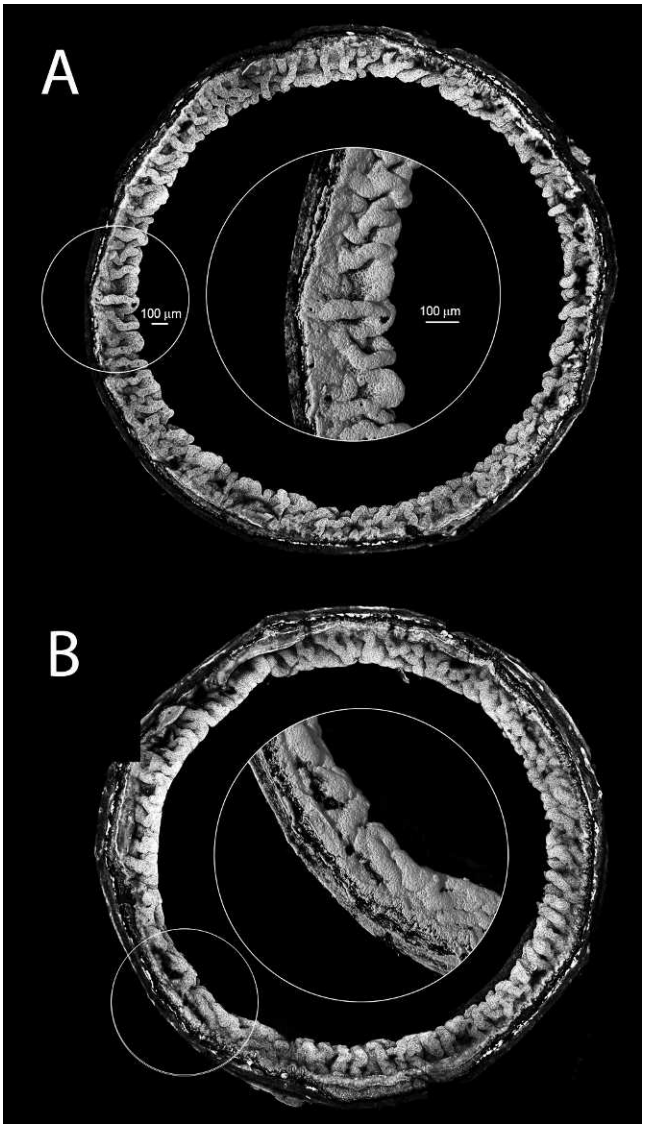

Figure 6. Anatomy of the ciliary body in 24-week-old WT and *Fbn2*$^{-/-}$ mice. Anatomy of intact ciliary bodies was reconstructed in three dimensions to examine the complex folding pattern of the ciliary epithelium. In WT mice (**A**), the ciliary epithelium is elaborately folded and the folds are predominantly radially oriented (see higher-magnification *central inset*). In *Fbn2*$^{-/-}$ animals (**B**), some regions of the ciliary body were folded normally, but in other areas (see *central inset*) folds were underdeveloped and circumferentially rather than radially oriented. Images are representative of four independent experiments. *Scale bars*: 100 μm.

epithelial border (marked by * in Figs. 7E, 7F) suggested that the differentiation process was no longer properly synchronized in cells approaching the lens equator.

Effects on Lens Size and Shape

The absence of Fbn2 disrupted the timing of lens fiber cell differentiation (Figs. 7E, 7F). We examined whether this, in turn, affected the growth of *Fbn2*$^{-/-}$ lenses or the curvature of their refractive surfaces. Lenses from *Fbn2*$^{-/-}$ mice were transparent and their internal refractive properties were indistinguishable from WT (Supplementary Fig. S4). However, careful analysis of lens size and shape revealed subtle differences between WT and *Fbn2*$^{-/-}$ mice. The anterior-posterior and equatorial diameters of the *Fbn2*$^{-/-}$ lenses were consistently smaller than WT. In WT lenses, the radius of curvature of the anterior lens surface was always significantly greater than the radius of the posterior surface. However, the radii of the anterior and posterior surfaces were indistinguishable in *Fbn2*$^{-/-}$ lenses (Fig. 8). Thus, in the absence of Fbn2, lenses were significantly smaller and more spherical.

Discussion

In this study, absence of *Fbn2* was associated most obviously with significant malformations of the iris. Fewer than 20% of *Fbn2*$^{-/-}$ eyes had morphologically normal irides. In contrast, approximately 37% had complete coloboma and 43% had dyscoric or eccentric pupils. In humans, off-centered or misshapen pupils are usually classified as "partial" coloboma. By this definition, iridal coloboma (complete or partial) was detected in approximately 80% of *Fbn2*$^{-/-}$ eyes. Coloboma is not uncommon in transgenic or knockout mice but it is unusual to find coloboma that involves the iris exclusively.[35] In the mouse eye, coloboma of the iris is generally found in conjunction with abnormalities of the posterior segment (choroid, retina, optic nerve head) and affected eyes are often microphthalmic. The presence of iris coloboma in an otherwise normally proportioned, intact globe may make *Fbn2*$^{-/-}$ mice a useful animal model for studying the cellular basis of this type of developmental ocular defect.

Iridal coloboma is a relatively rare condition in humans, with a prevalence of 2.3 per 100,000 births.[36] It occurs in isolation and as part of multisystem syndromes. According to Online Mendelian Inheritance in Man, iridal coloboma is a feature of more than 60 syndromes including Baraitser-Winter Syndrome 1 (MIM: 243310),[37] Temtamy syndrome (MIM 218340),[38] and Mowat Wilson syndrome (MIM: 235730).[39] Coloboma is also a principal feature of the CHARGE syndrome (coloboma, heart defects, atresia, retardation of growth, genital abnormalities, ear abnormalities; MIM: 214800).

It is generally accepted that "typical" colobomata (i.e., those located in the inferior quadrant of the eye) result from delayed or incomplete fusion of the optic fissure during embryonic development.[40,41] The optic fissure arises as an invagination of the ventral surface of the embryonic optic vesicle and is the opening through which mesenchymal cells enter the eye. These cells give rise to the vascular elements (tunica vasculosa lentis and PM) that temporarily surround and nourish the lens. The fissure normally closes during the fifth to seventh week of fetal development in humans[40] and between E11 and E13 in mice.[42] Failure of the fissure to close may result in coloboma of any of the structures it traverses. Fissure closure involves the orchestrated activity of a complex network of genes operating both within the eye and in the surrounding mesenchyme.[40] A number of genes, among them transcription factors, such as Vax1,[43] Vax2,[44] Pax6,[45] and Pitx2,[46] have been shown to play important roles in this process. In most cases, however, the downstream targets of these genes are not known. The observation that complete or partial iridal coloboma is common in *Fbn2*$^{-/-}$ mice suggests that *Fbn2* plays a previously unsuspected role in optic fissure closure. In situ hybridization experiments have shown that *Fbn2* expression is evident in the mesenchyme by E12.5.[25] Strong expression of *Fbn2* was also noted in the nonpigmented inner layer of the optic cup by E16.5. *Fbn2* expression was restricted to cells near the lip of the optic cup in a cell population that eventually gives rise to the NPCE. The restricted distribution of *Fbn2* mRNA transcripts may be of significance because the colobomata did not involve the posterior segment of the eye, suggesting a localized fusion

Investigative Ophthalmology & Visual Science

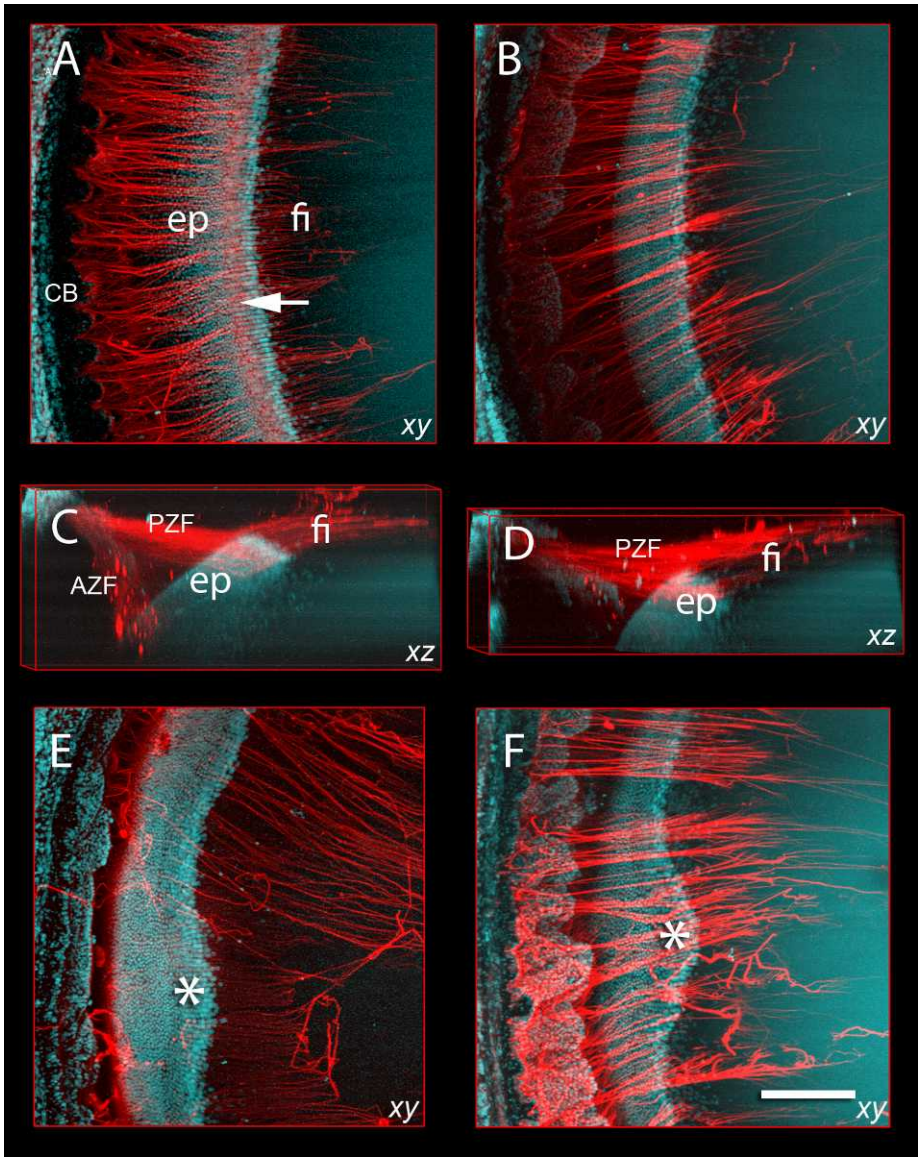

Figure 7. Zonular organization in 1-month-old WT and *Fbn2*$^{-/-}$ mice imaged from the posterior aspect. In WT mice (**A**), Magp1-positive zonular fibers (*red*) extend from the ciliary body (CB) to the lens equator. There are two prominent sets of zonular fibers (anterior zonular fibers [AZF] and posterior zonular fibers [PZF]) which attach to the lens on either side of the equator. The arrangement of the AZF and PZF in WT mice is best appreciated in *xz* projections of the data stack (**C**). The PZFs attach to the lens surface at the fibrillar girdle (*arrow* in [**A**]). The edge of the lens epithelium is defined by the absence of Draq5 nuclear staining (*light blue*). The fibrillar girdle is located at the edge of the lens epithelium, where epithelial cells (ep) differentiate into fiber cells (fi). In *Fbn2*$^{-/-}$ eyes (**B**, **D**–**F**), the arrangement of the zonular fibers is disturbed. In mildly affected cases (**B**), the AZFs are depleted in number (see also *xz* view shown in [**D**]) and many PZFs terminate posterior to the fibrillar girdle. In some cases, the zonules are profoundly disturbed (**E**, **F**). This is associated with de-synchronization of lens fiber differentiation, as indicated by the undulations in the epithelial border. In some regions the epithelium bulges beyond the equator (*), signifying a delay in fiber cell differentiation. Images are representative of six independent experiments. *Scale bar*: 200 μm.

deficit near the anterior lip of the fissure. Future studies will address the role of *Fbn2* in optic fissure closure in more detail.

Much progress has been made in identifying the molecules that trigger lens fiber cell differentiation. Various signaling pathways play a role, most notably the FGF pathway.[47] Less well understood, however, are the mechanisms that specify the location of the epithelial margin (i.e., the point on the lens surface where fiber cell differentiation begins). We have pointed out previously that the zonular apparatus is well positioned to serve such a role.[25] Fibrillins, the main structural component of the ciliary zonule, are known to bind and regulate the bioavailability of members of the TGFβ superfamily, including bone morphogenetic proteins, which have previously been implicated in fiber differentiation.[48] The current findings are consistent with the notion that the ciliary zonule may play a role in modulating lens growth. In *Fbn2*$^{-/-}$ mice, the zonular apparatus was disturbed. In particular, the attachment points of the zonular fibers on the lens surface were mislocated. In cases in which the zonules were particularly disorganized, the synchronized differentiation of the underlying fiber cells was affected.

Lenses from *Fbn2*$^{-/-}$ mice were smaller than WT and their surfaces were more spherical, although such changes could be independent of zonule effects, as the overall weight of *Fbn2*$^{-/-}$ mice was significantly reduced compared with WT. We note that in humans, mutations in *FBN1* lead to MFS and autosomal

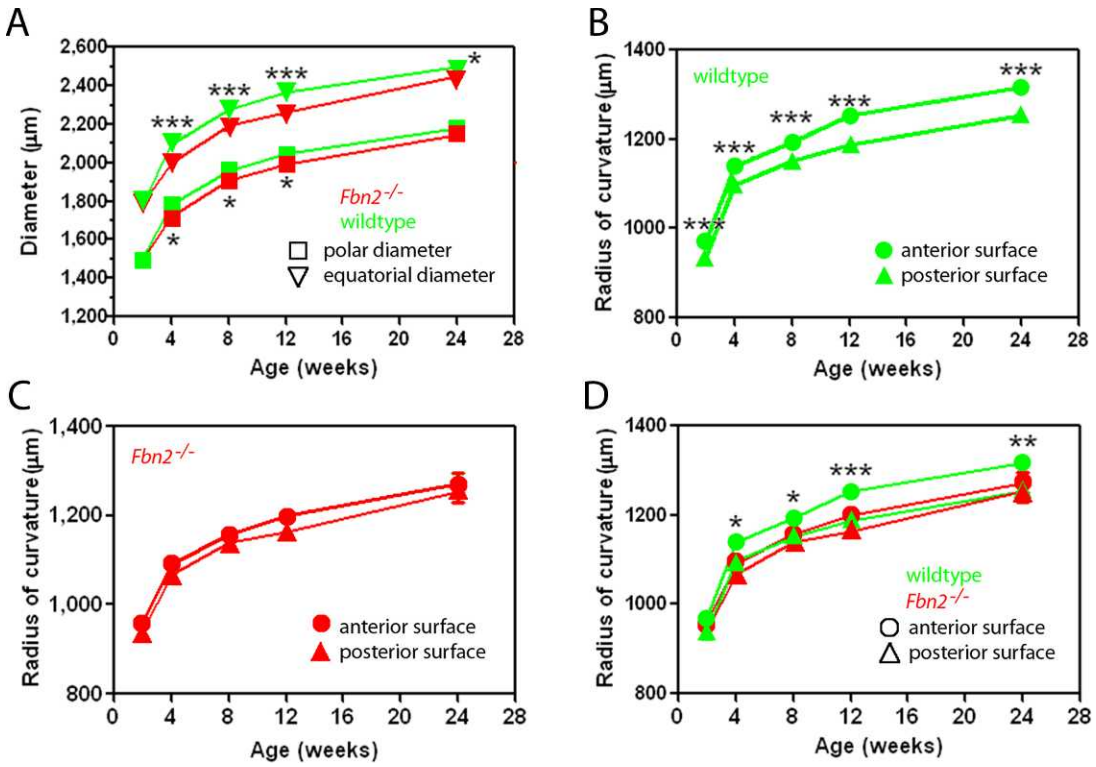

Figure 8. A comparison of lens size and shape in WT and *Fbn2*$^{-/-}$ mice. The equatorial and polar dimensions of the lens are significantly reduced in comparison to age-matched *Fbn2*$^{-/-}$ animals (**A**). In WT mice, the radius of curvature of the anterior lens face is significantly greater than the posterior face (**B**). In contrast, in *Fbn2*$^{-/-}$ mice, the radii of the two faces are statistically indistinguishable at all ages (**C**). Comparative data are shown in (**D**), illustrating a significant decrease in the anterior radius of curvature of WT in comparison to age-matched *Fbn2*$^{-/-}$ lenses. Data represent mean ± SEM for $n = 4$ animals (eight eyes) of each genotype at each age. *Error bars* fall within the data symbols. $^{*}P < 0.05$; $^{**}P < 0.01$; $^{***}P < 0.001$.

dominant Weill Marchesani syndrome, two conditions in which the lens is considerably smaller and more spherical than usual. Fibrillin-1-null mice die shortly after birth, precluding their use in ocular studies. However, a conditional *Fbn1* allele was generated recently[49] and, in conjunction with the *Fbn2*$^{-/-}$ mice used in the present study, should allow the role of fibrillins (individually and collectively) in fiber cell differentiation and lens growth to be tested explicitly.

All *Fbn2*$^{-/-}$ eyes with complete coloboma had persistent PMs. In humans, persistent PM is not uncommon in newborns.[50] Usually, the condition resolves without medical intervention but sometimes surgery is necessary.[51] In *Fbn2*$^{-/-}$ mice, the membrane was present at the lens surface directly beneath the gap in the notched iris. The persistent PM consisted of a microfibril-rich matrix and residual elements of the perilenticular capillary system. The observation that the PM regressed normally beneath intact iris but was retained in the notched region implies that the iris may play an active role in the regression of the PM. In mice, the PM normally regresses during the first 2 postnatal weeks,[33] although the mechanism is not completely understood. Experiments with macrophage-depleted animals have suggested that macrophages induce apoptosis in PM endothelial cells.[52,53] Other studies, however, have suggested a paracrine role for lens-derived BMP4.[54] Alternatively, it has been proposed that regression is triggered when the iris gains the ability to contract and, in so doing, influences blood flow in the underlying PM vessels.[55] The latter explanation may be most consistent with the current findings where regression did not occur in the absence of overlying iridal tissue.

Although *Fbn2* appears to be the dominant fibrillin transcript expressed during early development of the mouse eye, this may not necessarily be the case in humans, where proteomic analysis of the ciliary zonule has thus far identified only FBN1.[56] If *Fbn2* is not expressed at comparable levels in the murine and human eye, it may explain why mice lacking *Fbn2* have a high incidence of anterior segment pathology, whereas human patients with CCA are apparently affected only infrequently. In MFS, the iris is generally hypoplastic, leading to a transillumination defect.[57] In many cases, the ciliary body is also underdeveloped and the pupil miotic. Indeed, such defects often complicate corrective intraocular surgery for MFS. Thus, the high incidence of iris malformations in *Fbn2*$^{-/-}$ mice is, in some regard, more reminiscent of the ocular presentation of MFS than CCA. As a result, the *Fbn2*$^{-/-}$ mice may also prove useful for modeling intraocular sequelae of MFS.

Acknowledgments

The authors thank Russell Knutsen for his expert husbandry of the mice.

Supported by National Institutes of Health Grants EY09852 (SB), and HL53325 and HL74138 (RPM), Core Grant for Vision Research P30 EY02687; and an unrestricted grant to the Department of Ophthalmology and Visual Sciences from Research to Prevent Blindness. *Fbn2*$^{-/-}$ mice were generously provided by Francesco Ramirez, Mount Sinai School of Medicine, New York, New York.

Disclosure: **Y. Shi**, None; **Y. Tu**, None; **R.P. Mecham**, None; **S. Bassnett**, None

References

1. Sakai LY, Keene DR, Engvall E. Fibrillin, a new 350-kD glycoprotein, is a component of extracellular microfibrils. *J Cell Biol*. 1986;103:2499–2509.
2. Corson GM, Charbonneau NL, Keene DR, Sakai LY. Differential expression of fibrillin-3 adds to microfibril variety in human and avian, but not rodent, connective tissues. *Genomics*. 2004;83:461–472.
3. Jensen SA, Robertson IB, Handford PA. Dissecting the fibrillin microfibril: structural insights into organization and function. *Structure*. 2012;20:215–225.
4. Maumenee IH. The eye in the Marfan syndrome. *Trans Am Ophthalmol Soc*. 1981;79:684–733.
5. Beals RK, Hecht F. Congenital contractural arachnodactyly. A heritable disorder of connective tissue. *J Bone Joint Surg Am*. 1971;53:987–993.
6. Callewaert BL, Loeys BL, Ficcadenti A, et al. Comprehensive clinical and molecular assessment of 32 probands with congenital contractural arachnodactyly: report of 14 novel mutations and review of the literature. *Hum Mutat*. 2009;30:334–341.
7. Huggon IC, Burke JP, Talbot JF. Contractural arachnodactyly with mitral regurgitation and iridodonesis. *Arch Dis Child*. 1990;65:317–319.
8. Bass HN, Sparkes RS, Crandall BF, Marcy SM. Congenital contractural arachnodactyly, keratoconus, and probable Marfan syndrome in the same pedigree. *J Pediatr*. 1981;98:591–593.
9. Bawle E, Quigg MH. Ectopia lentis and aortic root dilatation in congenital contractural arachnodactyly. *Am J Med Genet*. 1992;42:19–21.
10. Rebelo CC, Furtado JM, Honjo RS, et al. Iris coloboma, blepharophimosis, arachnodactyly, joint contractures: Beals syndrome and Van den Ende-Gupta syndrome phenotypic similarities. *Clin Dysmorphol*. 2009;18:142–144.
11. Snape KM, Fahey MC, McGillivray G, Gupta P, Milewicz DM, Delatycki MB. Long-term survival in a child with severe congenital contractural arachnodactyly, autism and severe intellectual disability. *Clin Dysmorphol*. 2006;15:95–99.
12. Takaesu-Miyagi S, Sakai H, Shiroma T, Hayakawa K, Funakoshi Y, Sawaguchi S. Ocular findings of Beals syndrome. *Jpn J Ophthalmol*. 2004;48:470–474.
13. Anderson RA, Koch S, Camerini-Otero RD. Cardiovascular findings in congenital contractural arachnodactyly: report of an affected kindred. *Am J Med Genet*. 1984;18:265–271.
14. Gallego-Pinazo R, Lopez-Lizcano R, Millan JM, Arevalo JF, Mullor JL, Diaz-Llopis M. Beals-Hecht syndrome and choroidal neovascularization. *Clin Ophthalmol*. 2010;4:845–847.
15. Gupta PA, Putnam EA, Carmical SG, et al. Ten novel FBN2 mutations in congenital contractural arachnodactyly: delineation of the molecular pathogenesis and clinical phenotype. *Hum Mutat*. 2002;19:39–48.
16. Babcock D, Gasner C, Francke U, Maslen C. A single mutation that results in an Asp to His substitution and partial exon skipping in a family with congenital contractural arachnodactyly. *Hum Genet*. 1998;103:22–28.
17. Maslen C, Babcock D, Raghunath M, Steinmann B. A rare branch-point mutation is associated with missplicing of fibrillin-2 in a large family with congenital contractural arachnodactyly. *Am J Hum Genet*. 1997;60:1389–1398.
18. Hertwig P. Neue Mutationen und Koppelungsgruppen bei der Hausmaus. *Z Indukt Abstamm Vererbungsl*. 1942;80:220–246.
19. Johnson KR, Cook SA, Zheng QY. The original shaker-with-syndactylism mutation (sy) is a contiguous gene deletion syndrome. *Mamm Genome*. 1998;9:889–892.
20. Dixon MJ, Gazzard J, Chaudhry SS, Sampson N, Schulte BA, Steel KP. Mutation of the Na-K-Cl co-transporter gene Slc12a2 results in deafness in mice. *Hum Mol Genet*. 1999;8:1579–1584.
21. Chaudhry SS, Gazzard J, Baldock C, et al. Mutation of the gene encoding fibrillin-2 results in syndactyly in mice. *Hum Mol Genet*. 2001;10:835–843.
22. Miller G, Neilan M, Chia R, et al. ENU mutagenesis reveals a novel phenotype of reduced limb strength in mice lacking fibrillin 2. *PLoS One*. 2010;5:e9137.
23. Browning VL, Chaudhry SS, Planchart A, Dixon MJ, Schimenti JC. Mutations of the mouse Twist and sy (fibrillin 2) genes induced by chemical mutagenesis of ES cells. *Genomics*. 2001;73:291–298.
24. Arteaga-Solis E, Gayraud B, Lee SY, Shum L, Sakai L, Ramirez F. Regulation of limb patterning by extracellular microfibrils. *J Cell Biol*. 2001;154:275–281.
25. Shi Y, Tu Y, De Maria A, Mecham RP, Bassnett S. Development, composition, and structural arrangements of the ciliary zonule of the mouse. *Invest Ophthalmol Vis Sci*. 2013;54:2504–2515.
26. Weinbaum JS, Broekelmann TJ, Pierce RA, et al. Deficiency in microfibril-associated glycoprotein-1 leads to complex phenotypes in multiple organ systems. *J Biol Chem*. 2008;283:25533–25543.
27. Combs MD, Knutsen RH, Broekelmann TJ, et al. Microfibril-associated glycoprotein 2 (MAGP2) loss-of-function has pleiotropic effects in vivo. *J Biol Chem*. 2013;288:28869–28880.
28. Bassnett S, Shi Y. A method for determining cell number in the undisturbed epithelium of the mouse lens. *Mol Vis*. 2010;16:2294–2300.
29. Charbonneau NL, Dzamba BJ, Ono RN, et al. Fibrillins can co-assemble in fibrils, but fibrillin fibril composition displays cell-specific differences. *J Biol Chem*. 2003;278:2740–2749.
30. Shiels A, King JM, Mackay DS, Bassnett S. Refractive defects and cataracts in mice lacking lens intrinsic membrane protein-2. *Invest Ophthalmol Vis Sci*. 2007;48:500–508.
31. Shi Y, De Maria A, Bennett T, Shiels A, Bassnett S. A role for epha2 in cell migration and refractive organization of the ocular lens. *Invest Ophthalmol Vis Sci*. 2012;53:551–559.
32. Christensen AE, Fiskerstrand T, Knappskog PM, Boman H, Rodahl E. A novel ADAMTSL4 mutation in autosomal recessive ectopia lentis et pupillae. *Invest Ophthalmol Vis Sci*. 2010;51:6369–6373.
33. Ito M, Yoshioka M. Regression of the hyaloid vessels and pupillary membrane of the mouse. *Anat Embryol (Berl)*. 1999;200:403–411.
34. Napier HR, Kidson SH. Proliferation and cell shape changes during ciliary body morphogenesis in the mouse. *Dev Dyn*. 2005;233:213–223.
35. Chang L, Blain D, Bertuzzi S, Brooks BP. Uveal coloboma: clinical and basic science update. *Curr Opin Ophthalmol*. 2006;17:447–470.
36. Bermejo E, Martinez-Frias ML. Congenital eye malformations: clinical-epidemiological analysis of 1,124,654 consecutive births in Spain. *Am J Med Genet*. 1998;75:497–504.
37. Baraitser M, Winter RM. Iris coloboma, ptosis, hypertelorism, and mental retardation: a new syndrome. *J Med Genet*. 1988;25:41–43.
38. Temtamy SA, Salam MA, Aboul-Ezz EH, Hussein HA, Helmy SA, Shalash BA. New autosomal recessive multiple congenital abnormalities/mental retardation syndrome with craniofacial dysmorphism absent corpus callosum, iris colobomas and connective tissue dysplasia. *Clin Dysmorphol*. 1996;5:231–240.
39. Mowat DR, Croaker GD, Cass DT, et al. Hirschsprung disease, microcephaly, mental retardation, and characteristic facial features: delineation of a new syndrome and identification of a locus at chromosome 2q22-q23. *J Med Genet*. 1998;35:617–623.

40. Gregory-Evans CY, Williams MJ, Halford S, Gregory-Evans K. Ocular coloboma: a reassessment in the age of molecular neuroscience. *J Med Genet*. 2004;41:881–891.
41. Onwochei BC, Simon JW, Bateman JB, Couture KC, Mir E. Ocular colobomata. *Surv Ophthalmol*. 2000;45:175–194.
42. Hero I. The optic fissure in the normal and microphthalmic mouse. *Exp Eye Res*. 1989;49:229–239.
43. Hallonet M, Hollemann T, Pieler T, Gruss P. Vax1, a novel homeobox-containing gene, directs development of the basal forebrain and visual system. *Genes Dev*. 1999;13:3106–3114.
44. Barbieri AM, Broccoli V, Bovolenta P, et al. Vax2 inactivation in mouse determines alteration of the eye dorsal-ventral axis, misrouting of the optic fibres and eye coloboma. *Development*. 2002;129:805–813.
45. Baulmann DC, Ohlmann A, Flugel-Koch C, Goswami S, Cvekl A, Tamm ER. Pax6 heterozygous eyes show defects in chamber angle differentiation that are associated with a wide spectrum of other anterior eye segment abnormalities. *Mech Dev*. 2002; 118:3–17.
46. Gage PJ, Suh H, Camper SA. Dosage requirement of Pitx2 for development of multiple organs. *Development*. 1999;126: 4643–4651.
47. Lovicu FJ, McAvoy JW. Growth factor regulation of lens development. *Dev Biol*. 2005;280:1–14.
48. Boswell BA, Overbeek PA, Musil LS. Essential role of BMPs in FGF-induced secondary lens fiber differentiation. *Dev Biol*. 2008;324:202–212.
49. Cook JR, Smaldone S, Cozzolino C, et al. Generation of Fbn1 conditional null mice implicates the extracellular microfibrils in osteoprogenitor recruitment. *Genesis*. 2012;50:635–641.
50. Duke-Elder WS. *System of Ophthalmology*. St. Louis, MO: C.V. Mosby; 1964.
51. Kim SK, Quinn GE, Zaidman GW, Orlin SE. Congenital hyperplastic persistent pupillary membranes: a conservative approach in management. *J AAPOS*. 2005;9:391–393.
52. Lang RA, Bishop JM. Macrophages are required for cell death and tissue remodeling in the developing mouse eye. *Cell*. 1993;74:453–462.
53. Lang R, Lustig M, Francois F, Sellinger M, Plesken H. Apoptosis during macrophage-dependent ocular tissue remodelling. *Development*. 1994;120:3395–3403.
54. Kiyono M, Shibuya M. Bone morphogenetic protein 4 mediates apoptosis of capillary endothelial cells during rat pupillary membrane regression. *Mol Cell Biol*. 2003;23:4627–4636.
55. Morizane Y, Mohri S, Kosaka J, et al. Iris movement mediates vascular apoptosis during rat pupillary membrane regression. *Am J Physiol Regul Integr Comp Physiol*. 2006;290:R819–R825.
56. Cain SA, Morgan A, Sherratt MJ, Ball SG, Shuttleworth CA, Kielty CM. Proteomic analysis of fibrillin-rich microfibrils. *Proteomics*. 2006;6:111–122.
57. Maumenee IH. The eye in the Marfan syndrome. *Birth Defects Orig Artic Ser*. 1982;18:515–524.

Investigative Ophthalmology & Visual Science